Study of Transient Flow Structures in the Continuous Casting of Steel

Overview of Project Activities

This project was undertaken to improve understanding of fluid flow phenomena during the continuous casting of steel, which greatly affects quality and defects in the final steel product. It is part of a long-term effort to develop and apply comprehensive models of continuous casting, and is supported by experimental measurements and matching funds from the steel industry through the Continuous Casting Consortium at the University of Illinois.

Activities on this specific project (NSF Grant DMI-98-00274 from 1998 to 2001) began with development of computational models of steady and transient models of flow in the continuous casting nozzle and mold. The relative accuracy of these models is investigated through extensive comparison with laboratory measurements in water models, including particle image velocimetry, and with plant measurements conducted on continuous casting machines at the supporting steel companies. Next, extensive steady simulations are conducted to characterize multiphase fluid flow through the nozzle as a function of nozzle geometry and casting conditions. With the help of fundamental studies of bubble formation, the nozzle model is further applied to optimize argon injection to suggest guidelines to avoid nozzle clogging and to measure it using a "clogging index". Fully transient models of flow in the caster using Large Eddy Simulation are developed, evaluated, and applied to simulate flow in the mold. Then, the accuracy and relative advantages of the different models of fluid flow are compared with flow measurements in both water models and operating casters. Next, the models are applied to simulate three different phenomena associated with fluid flow in the mold: inclusion transport, heat transfer, and multiphase flow due to argon bubble injection. Guidelines are developed to predict optimal gas flow rates that should assist in designing better mold flow patterns to improve steel quality. Details of specific activities are discussed in the following sections according to the students who worked on them.

In addition to working on the research projects (and communicating the results through publishing book chapters, journal articles, conference presentations, online electronic articles and animations on two websites), semi-annual day-long meetings were held with industry representatives from the steel-related companies in the Continuous Casting Consortium (usually about 10 researchers from 7 different companies) to discuss the results of the individual projects, and to obtain feedback to benefit the students. Finally, the results from this work are incorporated into the short course to the steel industry (Brimacombe Continuous Casting Course, in Vancouver, Canada) which is presented annually by a team of 5 instructors including the PI of this project.

1. FLOW IN THE NOZZLE (Hua Bai)

A. Model of multiphase flow through continuous casting nozzles

Three-dimensional models have been developed to simulate steady flow in a variety of continuous casting nozzle geometries for single phase and multiphase conditions. Flow in the mold cavity, which is so important to quality, is governed by flow through the nozzle. Nozzle geometry is one of the casting operation variables that is both important to steel quality and easy to change. Flow in the nozzle is also important in its own right. Modeling

procedures for obtaining accurate quantitative predictions have been identified. These were obtained by first conducting mesh refinement and convergence studies.

An Eulerian multiphase model using the finite-difference program CFX has been applied to study the three-dimensional turbulent flow of liquid steel with argon bubbles in slide-gate tundish nozzles. The general governing equations that the model solves include mass and momentum balances for the liquid phase,

$$\frac{\partial(v_{li} f_l)}{\partial x_i} = 0 \tag{1}$$

$$\rho_l \frac{\partial(v_{lj} v_{li} f_l)}{\partial x_j} = -f_l \frac{\partial p_l}{\partial x_i} + \frac{\partial}{\partial x_j}\left[f_l(\mu_l + \mu_t)\left(\frac{\partial v_{li}}{\partial x_j} + \frac{\partial v_{lj}}{\partial x_i}\right)\right] + c_{lg}\left(v_{gi} - v_{li}\right) \tag{2}$$

and for the gas phase

$$\frac{\partial(v_{gi} f_g)}{\partial x_i} = 0 \tag{3}$$

$$\rho_g \frac{\partial(v_{gj} v_{gi} f_g)}{\partial x_j} = -f_g \frac{\partial p_g}{\partial x_i} + \frac{\partial}{\partial x_j}\left[f_g \mu_g\left(\frac{\partial v_{gi}}{\partial x_j} + \frac{\partial v_{gj}}{\partial x_i}\right)\right] + f_g(\rho_l - \rho_g) g_i + c_{lg}\left(v_{li} - v_{gi}\right) \tag{4}$$

where the indices i and j = 1,2,3 represent the x, y and z directions, $v_i = \{u, v, w\}$ are the velocity components in these three directions, the subscripts l and g donate the liquid and gas phases, f is volume fraction, ρ is density, ν is molecular viscosity and ν_t is the turbulent (or eddy) viscosity. Repeated indices imply summation. Because the density of the gas is 3-4 orders of magnitude smaller than that of the liquid and the gas fraction is small ($f_g \rho_g << f_l \rho_l$), turbulence in the gas phase is neglected. The standard, two-equation K-ε turbulence model is chosen for liquid phase turbulence, with modifications to account for the effect of liquid volume fraction. [1]

$$\rho_l \frac{\partial(f_l v_{lj} K)}{\partial x_j} = \frac{\partial}{\partial x_j}\left(f_l\left(\mu_l + \frac{\mu_t}{\sigma_k}\right)\frac{\partial K}{\partial x_j}\right) + \mu_t f_l \frac{\partial v_j}{\partial x_i}\left(\frac{\partial v_i}{\partial x_j} + \frac{\partial v_j}{\partial x_i}\right) - \rho_l f_l \varepsilon \tag{5}$$

$$\rho_l \frac{\partial(f_l v_{lj} \varepsilon)}{\partial x_j} = \frac{\partial}{\partial x_j}\left(f_l\left(\mu_l + \frac{\mu_t}{\sigma_\varepsilon}\right)\frac{\partial \varepsilon}{\partial x_j}\right) + C_1 \frac{\varepsilon}{K} \mu_t f_l \frac{\partial v_j}{\partial x_i}\left(\frac{\partial v_i}{\partial x_j} + \frac{\partial v_j}{\partial x_i}\right) - C_2 \rho_l f_l \frac{\varepsilon^2}{K} \tag{6}$$

The turbulent viscosity μ_t is calculated from the turbulent kinetic energy and dissipation by

$$\mu_t = C_\mu \rho_l \frac{K^2}{\varepsilon} \tag{7}$$

The above equations contain five empirical constants that appear to produce reasonable behavior for a wide range of flows [2] when given standard values as follows:

$$C_1 = 1.44,\ C_2 = 1.92,\ C_\mu = 0.09,\ \sigma_K = 1.00,\ \sigma_\varepsilon = 1.30$$

There is an obvious constraint that the volume fractions sum to unity

$$f_l + f_g = 1 \tag{8}$$

Equations 1-8 represent 12 equations with 13 unknowns (u, v, w, p, f for each phase, and μ_t, K, ε for liquid turbulence). The final equation needed to close the system is given by the simple constraint that both phases share the same pressure field: [1]

$$p_l = p_g = p \tag{9}$$

The last term of the momentum equations. Eqs. (2) and (4), accounts for inter-phase transfer of momentum between the liquid steel and the argon bubbles. Here, c_{lg} denotes the inter-phase momentum exchange coefficient, which is related to the relative velocity of the two phases by [3]

$$c_{lg} = \frac{3}{4}\frac{C_D}{D} f_g \rho_l \left| v_{li} - v_{gi} \right| \tag{10}$$

where D is the bubble diameter, assuming uniform-size spherical bubbles. The non-dimensional drag coefficient C_D is a function of the bubble Reynolds number, defined as Re_{bub}

$$Re_{bub} = \frac{\rho_l \left| v_l - v_g \right| D}{\mu_l} \tag{11}$$

The function $C_D(Re_{bub})$ is determined experimentally, and is known as the drag law [3]:

$$C_D = \frac{24}{Re_{bub}}\left(1 + 0.15 Re_{bub}^{0.687}\right) \tag{12}$$

This equation, known as the "Allen regime", is valid for $0 \le Re_{bub} \le 500$ -1000. Analysis of the results reveals that most bubbles in this study are in the Stokes regime, represented by the first term in Eq. 12. The domain and boundary conditions for this study are given in Figure A1.

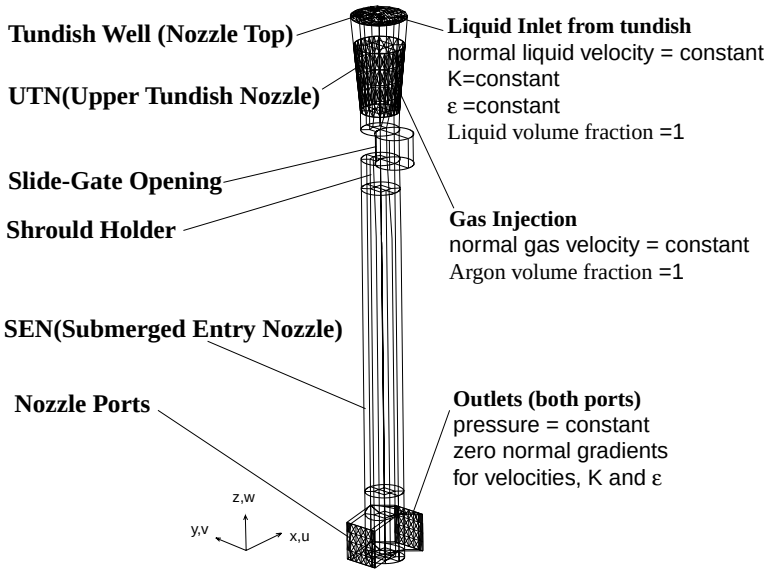

Fig. A1 Computational domain and boundary conditions for the slide-gate nozzle

B. Water Model Experiments and Particle Image Velocimetry for Model Validation

Because of the nearly equal kinematic viscosities of the liquid steel and water which determine the main flow characteristics, flow in the steel caster mold region can be studied using water models. In this work, we have conducted measurements of the flow in both a 0.4-scale water model at LTV Steel and a full-scale water model at AK Steel. Flow was measured both qualitatively, by visual observation and dye injection, and quantitatively using particle image velocimetry (PIV) measurements. The PIV experiments were conducted on 0.4-scale physical water models of the nozzle and mold, using the PIV system at LTV Steel Technical Center.

The PIV (Particle Image Velocimetry) system developed by DANTEC [4] was used to measure the velocity field at the plane of interest near the nozzle port. In PIV, a pulsed laser light sheet is used to illuminate a plane through the flow field which has been seeded with tracer particles small enough to accurately follow the flow. The positions of the particles in a 24x14 pixel field are recorded with a digital CCD (Charged Coupled Device) camera at each instant the light sheet is pulsed, yielding an "exposure". The images from two successive exposures are processed to match up individual particles and calculate the vector displacement of each. Knowing the time interval between the two exposures (1.5ms), the velocity of each particle can be calculated and the velocities are combined to produce an instantaneous velocity field. In this work, this procedure was repeated every 0.533 second to obtain the complete history of the fluctuating velocity field under nominally steady conditions. To obtain a time-averaged or "steady" velocity field, the results from 50 exposures were averaged.

The measurements have been applied to assess and validate the ability of flow models to simulate turbulent, multiphase flow through the continuous casting nozzle.[5, 6] and also flow in the mold.

C. Nozzle model application: parametric studies

The validated nozzle model has been applied to perform a large, systematic study of the effect of important operating parameters on flow exiting a typical slide-gate nozzle.[6, 7] Specifically, the jet characteristics (direction, speed, spread, etc.) exiting the nozzle ports are quantified for different operating parameters (nozzle bore diameter,

slide gate orientation, slide gate opening fraction, injected fraction of argon gas, steel flow rate, nozzle port angle, etc.). These results are a necessary first step in determining the important flow pattern in the mold. Flow conditions inside the nozzle are also important in their own right.

The standard conditions for this study are given in Table C1.

Table C1 Standard nozzle dimensions and operation conditions

Parameter	Standard Nozzle	
	SI Units	British units
Total nozzle length	1152.5 mm	45.37 in.
UTN top diameter	114 mm	4.49 in.
UTN length	241.5 mm	9.51 in.
Slide gate thickness	63 mm	2.48 in.
Slide gate diameter	78 mm	3.07 in.
Shroud holder thickness	100 mm	3.94 in.
SEN length	748 mm	29.45 in.
SEN bore diameter	78 mm	3.07 in.
SEN submerged depth	200 mm	7.87 in.
Port width x height	78mm x 78mm	3.07″ x 3.07″
Port thickness	29 mm	1.14 in.
Port angle (down)	15°	15°
Recessed bottom well depth	12 mm	0.47 in.
Gate orientation	90°	90°
Gate opening Linear fraction (F_L) Area fraction (F_A)	 50% 39%	 50% 39%
Casting speed (0.203m x 1.321m slab)	1.0 m/min	39.4 in./min (8″x52″slab)
Liquid volume flow rate	268.4 l/min	9.48 ft^3/min
Liquid mass flow rate	31.4 kg/s	2.07 ton/min
Argon injection flow rate Q_G (cold)	10 SLPM	0.35 SCFM
Argon injection (hot) volume fraction	16%	16%
Argon bubble diameter	1.0 mm	0.039 in.

D. Nozzle model application: nozzle clogging index

The model results were also presented for use at the steel plant as a "clogging index" to detect when nozzle clogging is present, before harmful flow defects occur. Clogging and other quality problems are indicated by level fluctuations in the mold, which result from the changes in the nozzle pressure drop and jets exiting the ports. The extent of clogging can be inferred by comparing the measured steel flow rate with the theoretical value for the given geometry, tundish depth, gas flow rate and percent gate opening. This is not easy because clogging initially increases flow before restricting it. The implications of these results have been extended in a comprehensive review on how to avoid nozzle clogging.[8]

E. Nozzle model application: argon gas flow optimization

The validated multiphase flow model of the nozzle was applied to perform over 150 simulations, in order to optimize argon gas injection levels in the nozzle for a range of practical conditions.[6] Specifically, the model results were processed (using simple inverse models) to quantify the minimum argon gas injection levels needed to avoid negative pressure in the nozzle, and thereby avoid air aspiration and the accompanying reoxidation, inclusion formation, and nozzle clogging. Practical guidelines on how to optimize argon injection are graphed for a range of casting conditions for a typical submerged entry nozzle geometry.

2. FLOW IN THE MOLD

A. Improved models of flow in continuous casting molds (S. Sivaramakrishnan; Q. Yuan)

Several different computational models have been developed to simulate turbulent fluid flow in continuous casting nozzles and molds, including both large eddy simulations (LES) and conventional time-averaged models, (such as K-ε).[9-11]

The time-dependent three-dimensional Navier-Stokes equations have been solved for the fluid velocity field.

$$\frac{\partial \mathrm{v}_i}{\partial x_i} = 0 \qquad (1)$$

$$\frac{D\mathrm{v}_i}{Dt} = -\frac{1}{\rho}\frac{\partial p}{\partial x_i} + \frac{\partial}{\partial x_j}\nu_{eff}\left(\frac{\partial \mathrm{v}_i}{\partial x_j} + \frac{\partial \mathrm{v}_j}{\partial x_i}\right) \qquad (2)$$

Some of the computations use no subgrid scale model, so may be termed course-grid DNS (direct numerical simulation). Other computations used the Smagorinsky eddy viscosity model [12] to represent the unresolved scales:

$$\nu_{eff} = \nu_0 + 0.01(\Delta x \Delta y \Delta z)^{2/3}\sqrt{\frac{\partial \mathrm{v}_i}{\partial x_j}\frac{\partial \mathrm{v}_i}{\partial x_j} + \frac{\partial \mathrm{v}_i}{\partial x_j}\frac{\partial \mathrm{v}_j}{\partial x_i}} \qquad (3)$$

The equations are discretized using the Harlow-Welch fraction step procedure on a staggered grid. Second order central differencing is used for the convection terms and the Crank-Nicolson scheme is used for the diffusion terms. The Adams-Bashforth scheme is used to discretize in time with second order accuracy. The implicit diffusion terms are solved using Alternative Line Inversion. The pressure Poisson equation is solved using a direct Fast Fourier

Transform solver. For parallelization, 1-D domain decomposition with MPI (Message Passing Interface) is utilized. The computation was conducted with a mesh consisting of 128 x 169 x 64 nodes in the x, y and z directions respectively. In a typical simulation (LES2) , the time-dependent equations were integrated for 175,000 time steps (140 seconds of real time). This computation takes 19.2 CPUs per time step on a Pentium III 750MHz PC or 39 days for 175,000 time steps.

The transient simulation LES1 was computed with a refined Large Eddy Simulation model and the Smagorinsky subgrid scale model, while LES2 used a fine 1.5 million-node grid with no turbulence model (so is really DNS). The time-average results from a conventional K-ε model are also performed and compared.

These models have been applied to increase understanding, identify and quantify some of the transient features of the flow field in the continuous casting nozzle, mold, and slag layers, and how they interact. Modeling procedures for obtaining quantitative predictions have been identified.

B. Plant benchmark experiments for continuous casting model validation (D.Creech, S. Sivaramakrishnan, and Steel Industry Researchers M. Assar (LTV) and R. O'Malley (AK))

Experiments have been conducted in the steel plants, including the operating casters at LTV Steel and AK Steel Mansfield. First, experiments were conducted at LTV Steel to obtain indirect insight into the flow pattern in the steel caster. LTV Steel personnel installed eletromagnetic sensors into the mold walls. These sensors measure flow velocity by comparing the time offset of the qualitative signal strength between a pair of probes a known distance apart. The installation of sensors is shown in Fig. B1. The accuracy of this experimental method was assessed using the transient computational flow models. In addition, the surface profile of the molten steel and flux layer interfaces was measured using "nail board experiments", wherein a series of steel nails and aluminum wires are dipped into the top surface (Fig. B2). The contour shape indicates the flow direction.

A comprehensive set of benchmark experiments were performed to quantify fluid flow, superheat dissipation, solidifying steel shell growth, heat transfer and microstructure during the continuous casting of stainless-steel slabs at the AK Steel caster in Mansfield, OH.[13] These experimental measurements, taken at virtually the same conditions, have further been applied to develop, calibrate, and validate mathematical models of both fluid flow and heat flow in continuous casting.[14] Three-dimensional turbulent flow of molten steel in the nozzle and the mold cavity is modeled with the finite difference code CFX 4.2,[1] using the standard K-ε turbulence model and a fixed, structured grid.

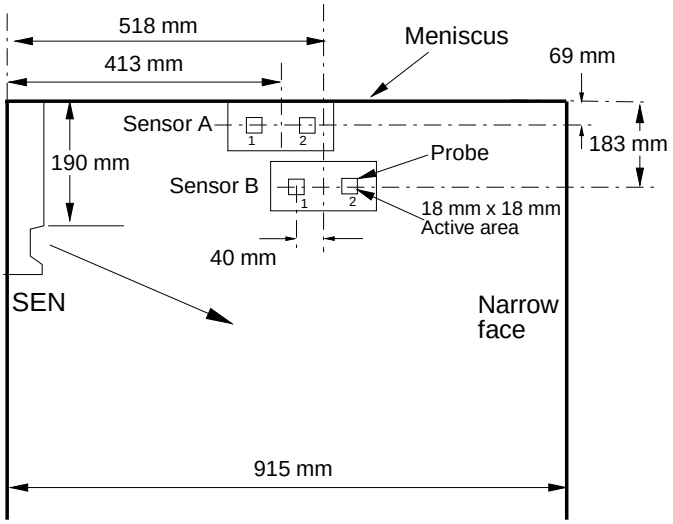

Fig. B1. Electromagnetic sensor locations (relative to steel caster dimensions)

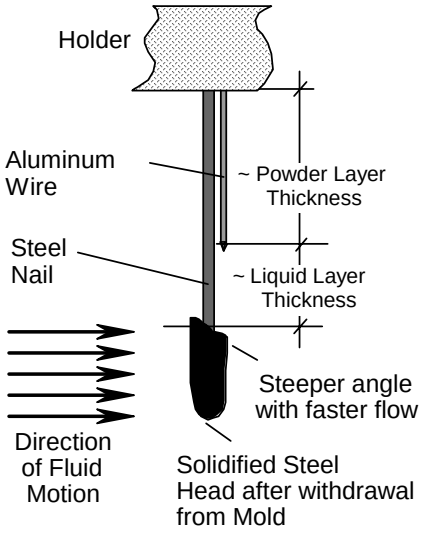

Fig. B2 Crude measurement of flux layer thickness and surface velocity

C. Validation of mold flow using water model PIV and plant measurements (S. Sivaramakrishnan; Q. Yuan)

To validate and assess the ability of flow models to simulate turbulent flow in molten metal processes, simulations were conducted for the same conditions as experiments using the PIV system at LTV Steel Technical Center. Both time-averaged (CFX) and transient (DNS / LES) models of flow in the mold were applied.[9-11, 15-18]

Flow fields in this molten metal process were compared for the first time using four different methodologies:

1) steady K-ε computations

2) transient LES computations

3) PIV measurements in a water model; and

4) electromagnetic sensor measurements in molten steel.

The experimental and simulation conditions for this study are in Table C1 and the domain is in Fig. C1 and B1.

Table C1 – Water model conditions

Tundish bath depth	400~410 mm
Nozzle length (total)	510 mm
UTN diameter	28 mm
Slide-gate diameter	28 mm
Slide-gate thickness	18 mm
Slide-gate orientation	90°
Slide-gate opening (FL)	52%
SEN submergence depth (top of port to top surface)	77± 3 mm
Bore (SEN) diameter	32 mm
Port width x height	31mm x 32mm
Port thickness	11 mm
Port angle, lower edge	15^o down
Port angle, upper edge	40^o down
Bottom well recess depth	4.8 mm
Water model length	950 mm
Water model width (steel caster width)	735 mm (72 in. full scale)
Water model thickness (steel caster thickness)	95 mm (top) to 65 mm (bottom) (9. in. full scale)
Outlets at bottom of mold domain (both halves)	3 round 35mm diameter outlets
Casting speed (model top)	0.633 m/min
Liquid flow rate through each port	3.53×10^{-4} m^3/s (5.6gal/min)
Average velocity at port	424 mm/s
Average jet angle at port	30^o down
Liquid kinematic viscosity	1.0×10^{-6} m^2/s
Gas injection	0%

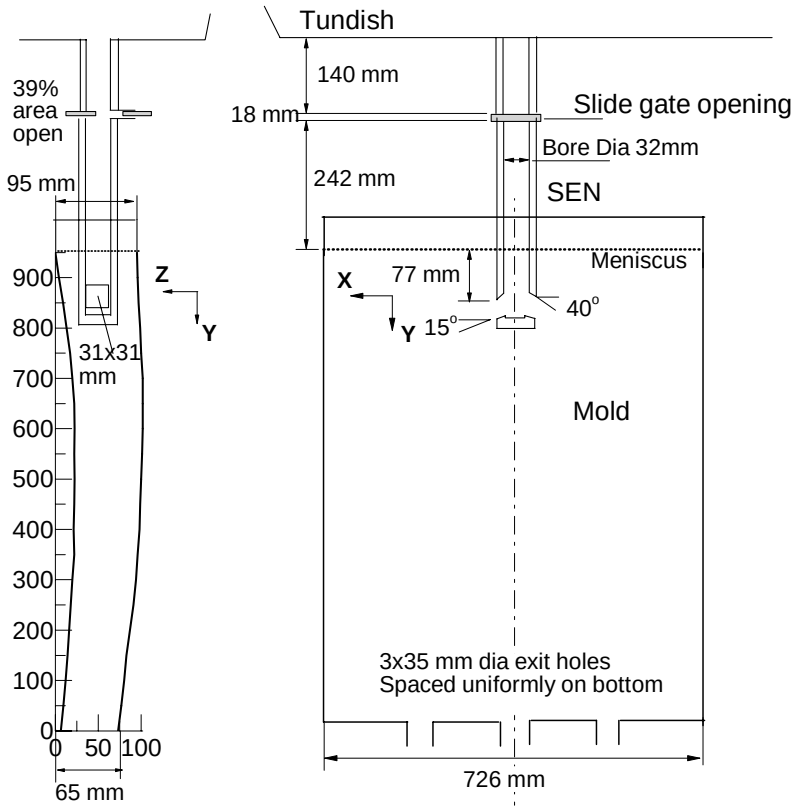

Fig. C1 – Schematics of the 0.4-scale water model domain.

D. Particle Transport in the Mold (Q. Yuan)

Particles such as alumina inclusions, which are carried in with the jet entering the mold, may cause serious defects in the final steel product if they are not able to float harmlessly into the top-surface slag layer. As an initial step to simulate particle transport, LES computations were extended to study both fluid flow and particle transport in the mold region of a full-scale water model[19] for conditions given in Table 1. The results are compared with water model measurements of both the flow velocities and the distribution and flotation removal of model inclusion particles.

Particle transport experiments[19] were performed in the water model by injecting 8000-30000 elliptical disk-shaped plastic beads with the water through the nozzle into the mold in each of at least five experiments. The density and size of the beads were chosen to match the vertical terminal velocity of 300mm alumina inclusions in molten steel. A screen was positioned near the top surface to trap the plastic beads and thereby simulate the removal of inclusion particles to the top surface. The average removal fraction was reported at different time intervals[19]. A hot-wire anemometer was used to measure the fluid velocity field.[20]

For inlet conditions on initial runs, the LES flow model adopted velocity profiles from a prior simulation of fully-developed turbulent-flow in a pipe, rotated to the 25˚ downward inlet angle observed in the water model. After quasi-steady flow conditions were achieved in the strand water model, a large group of 15,000 particles was introduced at random locations on the inlet plane over a 1.6 s time interval. Six further groups of 500 particles each

were then introduced every 2 seconds over 0.4s intervals. The particles were assumed to be spherical and were given initial velocities equal to the local instantaneous fluid velocity.

Each particle trajectory was tracked during the transient flow simulation using a Lagrangian approach, assuming a vertical buoyancy force according to the density difference and a drag force for particle Reynolds numbers up to 800.[21] The particle transport equation is:

$$v_{p,i} = \frac{dx_{p,i}}{dt} \tag{4}$$

$$\frac{dv_{p,i}}{dt} = \frac{18\rho\nu_0}{\rho_p d_p^{\,2}}\left(1+0.15\,\mathrm{Re}_p^{\,0.687}\right)\left(v_i - v_{p,i}\right) + \left(1-\frac{\rho}{\rho_p}\right)g_i \tag{5}$$

where: $$\mathrm{Re}_p = \frac{\left|\vec{v}_p - \vec{v}\right| d_p}{\nu_0} \tag{6}$$

The equations are integrated for each particle using a fourth order Runge-Kutta method at the same time as the velocity field is computed. The calculation This computation takes 2.4 additional CPUs per time step for 17500 particles or 5 additional days for 175000 time steps.

Table 1. Conditions for the full-scale water model measurements and simulation.

	Experiment	LES simulation
Nozzle port size /Inlet port size (x × y) (m)	0.051 × 0.056	0.051 × 0.056
Submergence depth (m)	0.150	0.150
Nozzle angle	25°	25°
Inlet jet angle	25°	25°
Mold /Domain height (m)	2.152	2.152
Mold /Domain width (m)	1.83	0.965
Mold /Domain thickness (m)	0.238	0.238
Average inlet flow rate (m^3/s)	0.00344	0.00344
Average inlet speed (m/s)	1.69	1.69
Fluid density (kg/m^3)	1000	1000
Casting speed (m/s)	0.0152	0.0152
Fluid kinematic viscosity (m^2/s)	1.0×10^{-6}	1.0×10^{-6}
Particle inclusion size (mm)	2 – 3	3.8 (diameter)
Particle inclusion density (kg/m^3)	988	988
Corresponding alumina inclusion diameter in steel caster (μm)	300	300

The domain for this work is given below:

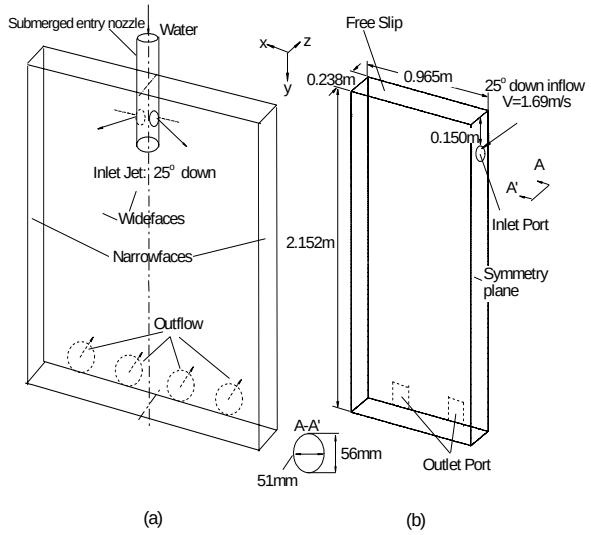

Figure: Schematic of (a) water model and (b) simulation domain.

E. Heat Transfer from an Impinging Jet (B. Zhao)

A separate set of computations was carried out to study the transient flow fields and rates of heat transfer under jets impinging on a solid surface. The objective of these studies was to evaluate the ability of LES to predict heat transfer rates for impinging jets. This is important for the prediction of shell thinning and breakouts in the continuous steel casting process.

Calculations were initially conducted to compare the results with available experimental data. Specifically, simulations were made of a circular air jet impinging orthogonally onto a cooled isothermal flat surface, for the conditions measured by Holworth and Gero, given in Tables E1 and E2 and shown in Fig. E1. The temperature of the jet is equal to that of the ambient air. The jet Reynolds number is varied from 5000 to 60,000. A turbulent flow field in a pipe is first computed. This is then prescribed as an inlet condition to the impinging jet computation. The radius of the domain, shown in Fig. E2, is taken to be 16 times the radius of the jet. At the outlet to the domain, the velocities are prescribed. A grid consisting of 128 x 64 x 128 cells was used for these computations.

The Smagorinsky [12] subgrid-scale model was used for these computations. The time dependent Navier-Stokes equations are solved with a finite-volume method with stagger location of velocities and pressures. The mesh is stretched in the radial direction. Instantaneous flow fields from a fully developed turbulent pipe flow simulation are prescribed as the inlet to the computational domain in a time-varying manner.

$\theta = \dfrac{T - T_p}{T_s - T_p}$ is the dimensionless temperature.

$t_c = d / V_b$ is the characteristic time, corresponds to 0.0013445s in the experiment.

The time step used in the simulation is 0.0001 time units, which means 10,000 time steps equals 1 time unit.

Table E1. Experimental and Simulation Conditions

d	Inlet diameter	$10\,mm$
Z	Nozzle to plate distance	$50\,mm$
T_p	Inlet temperature	$24 \sim 25°C$
T_a	Ambient temperature	Equals to T_p
T_s	Impingement surface temperature	$7 \sim 8°C$
ρ	Density of air	$1.2\ Kg/m^3$
μ	Molecule viscosity of air	$17.85\times10^{-6}\ Ns/m^2$
k	Thermal conductivity	$0.25\ W/mK$
Pr	Prandtl number	0.71
Re	Renolds number $V_b d/\nu$	5000
V_b	Inlet bulk velocity $\frac{4\dot{m}}{\pi d^2}$	$7.4375\,m/s$

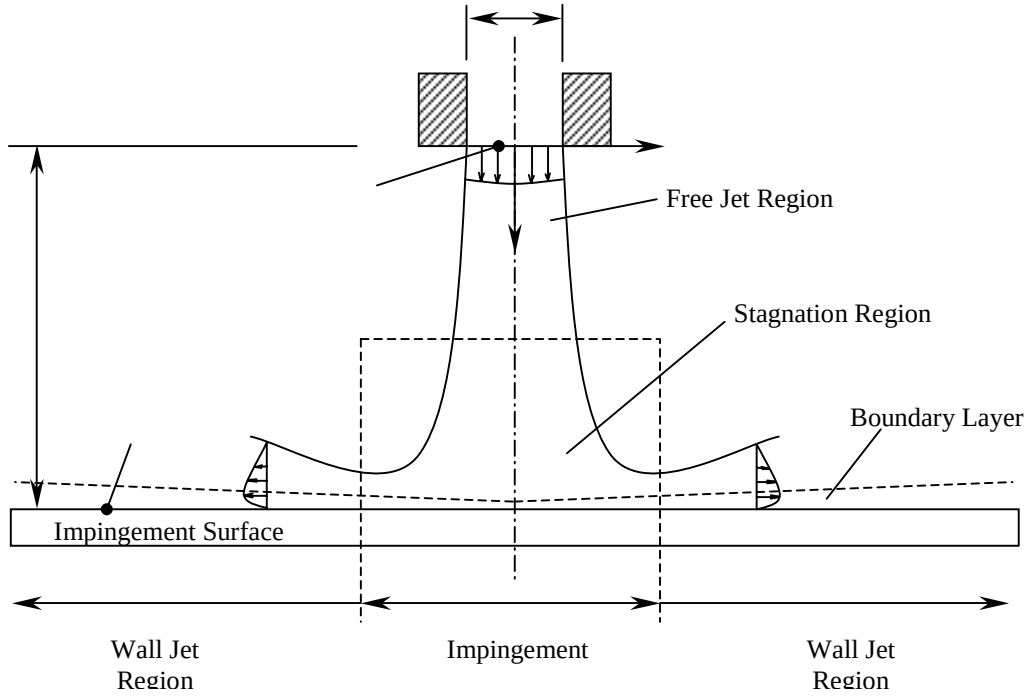

Fig. E1 Schematic of impinging jet

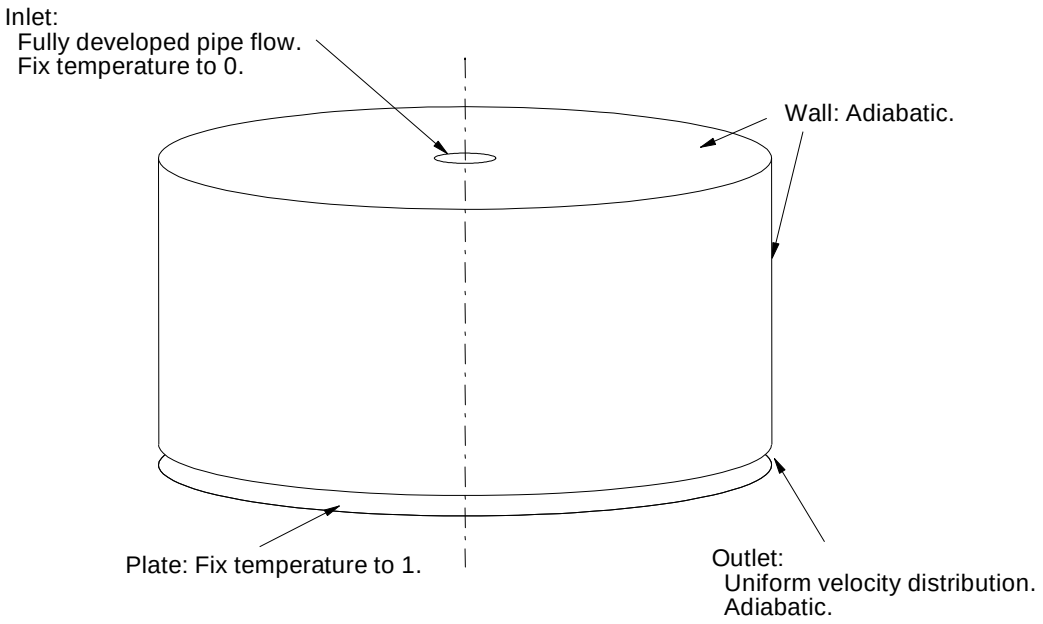

Fig. E2 Boundary conditions of the numerical simulation

Table E2. Fluid Properties for Impinging Jet Study

Temperature (°C)	Density ρ (kg/m^3)	Specific Heat C_p (J/kgK)	Thermal Conductivity k (W/mK)	Absolute Viscosity μ×106 (Ns/m2)	Kinematic Viscosity $\nu \times 10^6$ (m^2/s)
7.5	1.219	1011.4	0.242	17.75	14.6
24.5	1.1478	1012.5	0.254	18.44	16.1

Table 2.2 Fluid properties.

A new algorithm and LES code, CART3D is being developed to compute more general flows. This code is being applied to compute heat transfer in the flowing liquid pool in the actual continuous casting process. The heat transfer calculations are significantly more computationally intensive than the flow calculations, owing to the sharp gradients in the boundary layer at the solidifying interface, which controls heat losses from the liquid.

F. Multiphase Flow in the Mold: model development and validation (T. Shi)

Argon gas is often injected into the nozzle in order to prevent its clogging. This gas also has a great influence on flow in the strand. Increasing the amount of gas injection increases the buoyancy of the liquid jet, causing it to lift upward. Without gas, the classic "double roll" flow pattern is often produced, as studied in the previous section. Increasing the gas percentage above a critical level causes the flow pattern to change directions, forming a "single-roll" flow pattern, where the flow across the top surface is directed away from the SEN. This transition in flow patterns was studied using both water models and steady K-ε computations.

In this work, multiphase flow computations are compared with flow patterns observed in both a water model and an operating steel caster with argon gas injection. The model is extended to predict the flow pattern as a function of operating conditions, which can be used to optimize gas injection practice. A typical set of conditions studied is given in Table F1. This case was chosen because previous work had discovered discrepancies for these particular

conditions between the flow patterns found in a 0.4-scale water model and in the actual caster, as measured both by electromagnetic sensors in the mold wall and as inferred by the shape of the slag layer.[22]

To model two-phase flow, an additional set of momentum conservation equations was solved for the argon gas phase. Interphase coupling terms were added to the liquid momentum equations to account for the drag in proportion to the relative velocities of the liquid and bubble phases, which were generally in the Stokes or Allen regimes. The results depend greatly on the bubble size,[20] which in reality has a distribution that can evolve with the flow. In this work, these complex phenomena were treated by first characterizing the bubble size distribution as having eleven different discrete sizes, (0.5mm, 1.5mm, …, 10.5 mm) each with its own volume fraction, according to the Multiple Size Group model in CFX [1]. In this model, the average bubble velocity is related to the "Sauter" mean diameter of the distribution, in order to solve only a single additional set of gas momentum equations. Additional continuity equations are solved for each size group, to represent the size distribution. Furthermore, the initial bubble volume fractions, imposed at the nozzle port, were subjected to evolution, according to the binary breakup model of Luo and Svendsen [23], assuming a breakup coefficient of 0.1. Coalescence was assumed to be small (due to surface tension repulsion), by setting the coalescence coefficient [1] to 0.

The most difficult aspect of setting up the computational modeling was determination of the bubble size distribution. (Large numbers of small bubbles provide more drag than small numbers of large bubbles, so their buoyancy is able to exert more lift onto the flow pattern). The diameters of individual bubbles were measured from still photographs of the operating water model and compiled into a volume fraction distribution. Bubble sizes in the caster were estimated by extrapolating size distributions measured in a water model of a nozzle where vertical flow generated bubbles via shear. The results were adjusted for steel / argon properties by applying the mathematical model of Bai,[6] assuming about 200 active sites for gas emission from the 78 mm bore x 50 mm high cylindrical surface area of the porous ceramic wall. The computation begins by first solving for flow in the nozzle. Conditions at the exit plane of the nozzle port, including the velocity components, K, and ε distributions are used to define the inlet conditions for the strand simulation. The calculated flow pattern in the strand water model is compared with the velocity distribution measured using Particle Image Velocimetry.

The computational model was next applied to simulate the flow pattern measured in the steel caster for approximately the same conditions. The steel caster is different from the water model in several important ways. Changes to this simulation, given in Table 3 include:

-increasing the dimensions by a factor of 2.5 to simulate the full-scale geometry;

-increasing the inlet velocities by a factor of 1.581 (to simulate the actual casting speed rather than the velocities in the water model, which were scaled down according to the standard modified Froude criterion);

-replacing the domain bottom with a pressure boundary condition;

-changing the bubble distribution (Fig. 11); and

-changing the liquid properties.

The results are compared with indirect plant observations of the steel flow pattern, obtained in two ways. First, the surface shape of the liquid flux layer is measured by dipping nail boards through the molten flux and steel. In

addition, the signals from electromagnetic sensors inserted into the mold walls of the operating caster are evaluated to determine the flow direction. This comparison is used to evaluate the accuracy of both the water model and computational models.

Table F1. Multiphase Flow Model Conditions

	0.4-scale Water Model	Steel Caster
Mold Width x Thickness	730 x 80 mm	1854 x 228 mm
Mold / Strand Height	950 mm	open bottom
Nozzle Submergence Depth (top surface to top of port)	80 mm	165 mm (6.5 inch)
Nozzle Bore Inner Diameter	31 mm	80 mm
Port Wall Thickness	11mm	27.5 mm
Nozzle Port Height x Width	31 x 31 mm	78 x 78 mm
Nominal Vertical Angle of Port Edges	15° down	15° down
Jet Angle: vertical, horizontal	30˚ down 0˚	10.1˚ down 12.1˚
Average Inlet Velocities, V_x, V_z	0.358 m/s, 0.207 m/s	0.562 m/s, 0.324 m/s
Inlet Turbulent Kinetic Energy, K_o	0.044 m^2/s^2	0.193 m^2/s^2 avg.
Inlet Turbulence Dissipation Rate, ε_o	0.999 m^2/s^3	3.037 m^2/s^3 avg.
Liquid Density, ρ	1000 kg/m^3	7020 kg/m^3
Liquid Laminar Viscosity, μ_o	0.001 kg/m-s	0.0056 kg/m-s
Casting Speed, V_c	Froude similarity	14.8 mm/s (35''/min)
Liquid Flow Rate (whole slab)	0.0378 m^3/min	0.376 m^3/min
Gas Flow Rate (cold) (hot)	 3.71 SLPM	6.3 SLPM 34.9 SLPM
Gas Volume Fraction, f_{gas}	8.9 %	8.5%
Bubble diameter (avg)	2.43 mm	2.59 mm

G. Multiphase Flow in the Mold: Flow Pattern Optimization (T. Shi, L. Zhang)

Having validated the computational multiphase flow model, it was next applied to determine the upper limit for argon injection that still produces a stable double-roll flow pattern and avoids the detrimental transition flow pattern. Simulations were performed for a range of conditions, including different casting speeds (leading to different throughputs) and different argon injection rates. Figures are constructed to show the flow pattern as a function of typical operating conditions. Future work is needed to correlate the different flow patterns with defects, such as inclusion particle entrainment, in a quantitative manner. This is the subject of the current NSF Grant # DMI-01-15486.

3. REFERENCES

1. CFX 4.2, Report, AEA Technology, 1700 N. Highland Rd., Suite 400, Pittsburgh, PA 15241, 1998.

2. B.E. Launder and D.B. Spalding, "Numerical Computation of Turbulent Flows," Comp. Meth. Applied Mechanics and Engr., Vol. 13 (3), 1974, 269-289.

3. R. Clift, J.R. Grace and M.E. Weber, Bubbles, Drops, and Particles, Academic Press Inc., 1978.

4. Dantec Flow Technology, User's Guide, V. 2.01, 777 Corporate Drive, Mahwah, New Jersey 07430, 1998.

5. H. Bai and B.G. Thomas, "Turbulent Flow of Liquid Steel and Argon Bubbles in Slide-Gate Tundish Nozzles, Part I, Model Development and Validation," Metall. Mater. Trans. B, Vol. 32B (2), 2001, 253-267.

6. H. Bai, "Argon Bubble Behavior in Slide-Gate Tundish Nozzles During Continuous Casting of Steel Slabs," PhD Thesis, University of Illinois, 2000.

7. H. Bai and B.G. Thomas, "Turbulent Flow of Liquid Steel and Argon Bubbles in Slide-Gate Tundish Nozzles, Part II, Effect of Operation Conditions and Nozzle Design," Metall. Mater. Trans. B, Vol. 32B (2), 2001, 269-284.

8. B.G. Thomas and H. Bai, "Tundish Nozzle Clogging – Application of Computational Models," in Steelmaking Conf. Proc., Vol. 18, Iron and Steel Society, Warrendale, PA, (Baltimore, MD), 2001, 895-912.

9. B.G. Thomas and S.P. Vanka, "Study of Transient Flow Structures in the Continuous Casting of Steel," NSF Design & Manufacturing Grantees Conference, (Long Beach, CA), NSF, Washington, D.C., 1999.

10. B.G. Thomas and S.P. Vanka, "Study of Transient Flow Structures in the Continuous Casting of Steel," NSF Design & Manufacturing Grantees Conference, (Vancouver, Canada), NSF, Washington, D.C., 2000, 14p.

11. S.P. Vanka and B.G. Thomas, "Study of Transient Flow Structures in the Continuous Casting of Steel," NSF Design & Manufacturing Grantees Conference, (Jan. 7-10, Tampa, FL), NSF, Washington, D.C., 2001, 14p.

12. J. Smagorinsky, "General Circulation Experiments With the Primitive Equations, I. The Basic Experiment," Monthly Weather Review, Vol. 91, 1963, 99-164.

13. B.G. Thomas, R.J. O'Malley and D.T. Stone, "Measurement of temperature, solidification, and microstructure in a continuous cast thin slab," Modeling of Casting, Welding, and Advanced Solidification Processes, (San Diego, CA), TMS, Warrendale, PA, Vol. VIII, 1998, 1185-1199.

14. B.G. Thomas, R. O'Malley, T. Shi, Y. Meng, D. Creech, D. Stone, "Validation of Fluid Flow and Solidification Simulation of a Continuous Thin Slab Caster," in Modeling of Casting, Welding, and Advanced Solidification Processes, Vol. IX, Shaker Verlag GmbH, Aachen, Germany, (Aachen, Germany, August 20-25, 2000), 2000, 769-776.

15. B.G. Thomas, H. Bai, S. Sivaramakrishnan, S.P. Vanka, "Detailed Simulation of Flow in Continuous Casting of Steel Using K-ε, LES, and PIV," International Symposium on Cutting Edge of Computer Simulation of Solidification and Processes, (Osaka, Japan, Nov. 14-16, 1999), ISIJ, 1999, 113-128.

16. S. Sivaramakrishnan, H. Bai, B.G. Thomas, P. Vanka, P. Dauby, M. Assar, "Transient Flow Structures in Continuous Cast Steel," in Ironmaking Conference Proceedings, Vol. 59, ISS, Warrendale, PA, (Pittsburgh, PA), 2000, 541-557.

17. S. Sivaramakrishnan, B.G. Thomas and S.P. Vanka, "Large Eddy Simulation of Turbulent Flow in Continuous Casting of Steel," in Materials Processing in the Computer Age, Vol. 3, V. Voller and H. Henein, eds., TMS, Warrendale, PA, 2000, 189-198.

18. S. Sivaramakrishnan, "Transient Fluid Flow in the Mold and Heat Transfer Through the Molten Slag Layer in Continuous Casting of Steel," M.S. Thesis, University of Illinois, 2000.

19. R.C. Sussman, M. Burns, X. Huang, B.G. Thomas, "Inclusion Particle Behavior in a Continuous Slab Casting Mold," in 10th Process Technology Conference Proc., Vol. 10, Iron and Steel Society, Warrendale, PA, (Toronto, Canada, April 5-8, 1992), 1992, 291-304.

20. B.G. Thomas, X. Huang and R.C. Sussman, "Simulation of Argon Gas Flow Effects in a Continuous Slab Caster," Metall. Trans. B, Vol. 25B (4), 1994, 527-547.

21. L. Shiller and A. Naumann, "Uber die grundlegenden Berechungen bei der Schwerkraftaufbereitung," Ver. Deut. Ing., Vol. 77, 1933, 318.

22. M.B. Assar, P.H. Dauby and G.D. Lawson, "Opening the Black Box: PIV and MFC Measurements in a Continuous Caster Mold," in Steelmaking Conf. Proc., Vol. 83, ISS, Warrendale, PA, (Pittsburgh, PA), 2000, 397-411.

23. H. Luo and H.F. Svendsen, "Theoretical model for drop and bubble breakup in turbulent dispersions," AICHE J., Vol. 42 (5), 1996, 1225-1233.